J. Fluid Mech. (1991), *vol.* 225, *pp.* 101–120
Printed in Great Britain

Numerical simulations of the nonlinear kink modes in linearly stable supersonic slip surfaces

By JEFFREY A. PEDELTY† AND PAUL R. WOODWARD
Department of Astronomy *and* Minnesota Supercomputer Institute, University of Minnesota, Minneapolis, MN 55455, USA

(Received 13 March 1989 and in revised form 6 July 1990)

We have performed high-resolution numerical simulations of supersonic slip surfaces to confirm and illuminate earlier analytic nonlinear stability calculations of such structures. This analytic work was in turn inspired by earlier computer simulations reported in Woodward (1985) and Woodward *et al.* (1987). In particular Artola & Majda (1987) examined the response of a supersonic slip surface to an incident train of small-amplitude nonlinear sound waves. They found analytic solutions which indicate that nonlinear resonance occurs at three angles of incidence which depend upon the Mach number of the relative motion. The two-dimensional simulations described here numerically solve this problem for a Mach-4 flow using the piecewise-parabolic method (Colella & Woodward 1984; Woodward & Colella 1984). The simulations show that sound waves incident at a predicted resonance angle excite nonlinear behaviour in the slip surface. At these angles the amplitude of the reflected waves is much greater than the incident wave amplitude (i.e. a shock forms). The observed resonance is fairly broad, but the resonance narrows as the strength of the incident waves is reduced.

The nature of the nonlinear kink modes observed in the simulations is similar to that discussed by Artola & Majda. Most of the modes move in either direction with speeds near the predicted value. Speeds of other than this value are observed, but the disagreement is not serious in view of the strongly nonlinear behaviour seen in the simulations but not treated in the analytic work. The stationary modes seen in the analytic results are perhaps observed as transient structures. They may eventually dominate the flow at late times (Woodward *et al.* 1987).

The role of the kink modes in the stability of slab jets is discussed, and it is argued that the stationary modes are more disruptive than the propagating modes.

1. Introduction

The study of supersonic fluid flows which contain shear layers is a fundamental problem for both mathematicians and physical scientists. The limit where the velocity change occurs in an infinitesimal distance, the so-called vortex sheet or slip surface approximation, provides a well-defined problem for mathematical analysis (Gerwin 1968). This approximation is also relevant to many interesting astrophysical situations, including the boundaries of jets which are observed to emanate from young stellar objects (Lada 1985), late-type stars (Hjellming & Johnston 1985), and active galactic nuclei (Bridle & Perley 1984).

The supersonic slip surface has been studied using the techniques of linear stability analysis by Miles (1958). The well-known result is that for fluids of equal density the

† Current address: Code 936, NASA Goddard Space Flight Center, Greenbelt, MD 20771.

motion is neutrally stable when the relative Mach number is greater than $2\sqrt{2}$. For speeds below this limit the analysis predicts exponentially growing modes.

Woodward (1986) has performed high-resolution numerical simulations of the nonlinear evolution of supersonic slip surfaces using the piecewise-parabolic method (PPM). These results demonstrated that a nonlinear instability occurs in flows that linear stability analysis predicts to have no growing modes. This instability is characterized by two pairs of nonlinear waves associated with a kink in the slip surface. Once generated these shock and rarefaction wave combinations grow nearly self-similarly with time. In the numerical simulations more than one kink and nonlinear wave system is generated. The wave systems move with different speeds and eventually interact. The interaction of the kinks and their nonlinear wave systems ultimately cause the slip surface to roll up. The final state of this instability is very similar to those observed by Woodward (1985) in linearly unstable slip surfaces, but occurs at a much later time.

In an effort to understand the behaviour demonstrated in these simulations, Artola & Majda (1987, hereinafter referred to as AM) have recently performed a nonlinear analytical study of the response of a supersonic slip surface (or vortex sheet) within a region of spatially uniform density to an incident sound wave train of very small amplitude. The AM study extended the linear analysis of Miles (1957). AM derived the solutions for small nonlinear perturbations of the slip surface which indicate that nonlinear resonance occurs at three angles of incidence which depend on the Mach number of relative motion. For these angles the perturbation expansions are simplified. The solution of the simplified equations shows that the amplitudes of the reflected and transmitted waves are much larger than the incident wave amplitude. At resonance these reflected and transmitted waves are a shock and rarefaction associated with a finite-amplitude kink in the slip surface. The resonant modes are designated $u_{\pm}$ and u_0 by AM. The $u_{\pm}$ modes move with equal and opposite velocities which are a function of the slip-surface Mach number, while the u_0 mode is stationary in the frame in which the fluid velocities are equal and opposite.

These kink modes may be the characteristic nonlinear responses observed in the slip-surface simulations of Woodward. The goal of the present study is to solve numerically the same type of problem solved analytically by AM, and to follow any growing modes well into the large-amplitude regime. The response of an equal-density, Mach-4 slip surface to a variety of impinging nonlinear sound wave trains is numerically computed using PPM. A demonstration of the existence of a resonance in the response of the slip surface supports the AM analysis. The numerical solutions also complement and extend the analytical work by revealing the dynamical properties of the kink modes in the fully nonlinear limit. The correspondence between the analytical work and the simulations also demonstrates that the kinks seen in the earlier simulations of Woodward were not spuriously generated by numerical errors.

It should be made clear that the word kink is used in this paper to describe a localized small-amplitude distortion of the slip surface, and does not refer to the large-scale bending of jets often seen in astrophysical contexts. For this paper the latter phenomenon will be referred to as large-scale bending or meandering.

2. Problem description

2.1. *Initial and boundary conditions*

The initial condition for all of the problems is an equilibrium slip surface. Cartesian geometry is used, with the slip surface defining the x-axis. The flow velocities above and below the slip surface are Mach 2, with no transverse velocity component. The density, ρ, the sound speed, c, are everywhere equal to 1. The pressures on either side of the slip surface are equal. The fluids are assumed to be ideal gases with the ratio of their specific heats, γ, equal to 5/3. Since PPM solves the Euler equations of ideal gas dynamics, the solution is free of scales set by, for example, viscosity or heat transfer. The distance unit is thus arbitrary, and the time unit is the interval required for a sound wave to travel one distance unit in the unperturbed gas.

A finite train of sound waves is set up in the flow above the slip surface. These waves travel at an angle ϑ toward the slip surface at the local velocity of sound, c. To produce this wave train a sinusoidal perturbation with wavelength λ is applied to the R_+ Riemann invariant. In the initial adiabatic flow R_+ is given by

$$R_+ = u + \frac{2c}{\gamma - 1},$$

where u is the component of the initial flow velocity perpendicular to the sound wave fronts. The value of λ used in all of the simulations is 0.125, while the amplitude of the R_+ perturbation varied between 1 and 50%. Since the Riemann invariants are advected at the local Lagrangian sound speed ρc (Courant & Friedrichs 1948), this perturbation will generate the desired sound waves. To make a finite wave train a Gaussian envelope in the dimension perpendicular to the slip surface is applied to the perturbation. This envelope reduces the R_+ perturbation at the slip surface by a factor $e^{-6} \approx 1/403$ from its peak value. The peak value of the perturbation is located a distance $3.5\lambda/\cos(\vartheta)$ above the slip surface.

The boundary conditions perpendicular to the slip surface are periodic, while on either side of the slip surface outflow boundary conditions are maintained. The length of the computational area along the slip surface is determined by the need to include one period of the incident sound wave train, and is given by $\lambda/\sin(\vartheta)$. The computational area is evenly zoned to a distance of $7\lambda/\cos(\vartheta)$ above and below the slip surface, while further from the slip surface the zones exponentially increase in size out to a distance of 3. In the present simulations signals do not have time to reach this boundary; thus the calculations are free from any signals induced by the outflow condition.

The grid is very fine, with $360^2 = 129600$ zones on either side of the slip surface, and is symmetric about the slip surface. The size of the regularly spaced zones is approximately 0.003 square, which resolves well the incident sound wave with approximately 40 zones per wavelength. The details of the zoning and initial conditions for each of the simulations are listed in table 1.

2.2. *Numerical method*

The numerical method used to perform the flow simulations was a simplified version of the PPM, appropriate for flows with relatively weak shocks. Detailed descriptions of the full method are given by Colella & Woodward (1984) and Woodward (1986), and a comparison of the performance of PPM with several other modern methods is made by Woodward & Colella (1984).

Briefly, PPM is a second-order extension of the method of Godunov (1959), and

has grown out of the MUSCL scheme (van Leer 1979). It is a conservative scheme which updates the mass, momentum, and total energy in each computational zone by differencing time-averaged fluxes of these quantities which have been computed at the zone interfaces. The fluxes are obtained by solving Riemann problems (or shock-tube problems, Courant & Friedrichs 1948) which describe the nonlinear interaction of two uniform states of the flow. These states are determined using information from the proper domains of dependence of the two families of sound waves which reach the interface during a time step. Within these domains of dependence the quantities are averaged by using interpolated parabolic representations which have been constrained to be monotonically increasing or decreasing as appropriate.

No explicit interface tracking scheme is employed in these calculations. The boundary between the two velocity components is kept sharp by means of the contact discontinuity steepener present in PPM. This steepening algorithm is designed to detect physical contact discontinuities by testing for sufficiently large density contrasts unaccompanied by pressure jumps. The internal structure of such flow regions is steepened beyond that given by the usual monotonized interpolation parabolae produced by PPM.

The two-dimensional calculations were performed using a symmetrized sequence of one-dimensional calculations. These one-dimensional passes were performed using a Lagrangian step followed by a remapping onto the Eulerian grid.

The version of PPM used in these calculations uses the simplified dissipation mechanism described by Woodward (1986). This dissipation is designed to prevent spurious oscillations of the post-shock flow variables, and is applied only in shocked regions. In these regions the interpolated internal structure of the flow variables is blended with lower-order approximations. A simplified linear solution to the Riemann problem which does not involve iteration is also used (see figure 19 of Woodward 1986). These simplifications reduce execution times, and are appropriate for flows that do not include strong shocks. In practice this restriction is not too severe and includes flows with Mach numbers up to approximately 8, well above the value of Mach 4 in the present simulations.

3. Analytical expectations

For the Mach-4 slip-surface configuration described above, the AM analysis predicts that for three angles of incidence the sound wave train will excite nonlinear resonant behaviour. The three kink modes are designated $u_{\pm}$ and u_0. The $u_{\pm}$ kink modes move along the slip surface with velocities of $\pm \Gamma c$, where Γ is a function of the Mach number, M, of the two fluids

$$\Gamma = [1+M^2-(1+4M^2)^{\frac{1}{2}}]^{\frac{1}{2}},$$

and c is the velocity of sound in the undisturbed fluid. For a relative Mach number of 4, or $M = 2$, the value of Γ is 0.936. The u_0 kink mode is stationary in the frame of reference of the simulations in which the fluids have equal and opposite velocities.

The angle of incidence necessary to excite the u_- kink mode in a Mach-4 slip surface is given by the condition that the phase velocity of the incident wavefronts along the slip surface is $\Gamma c = 0.936c$. Simple geometrical considerations show that the resonant angle of incidence, ϑ, satisfies the relation

$$\sin(\vartheta) = \frac{1}{M+0.936}.$$

ϑ (deg.)	Number of x-zones	x maximum	Number of uniform y-zones	y maximum in uniform zones	Phase velocity of wave train along slip surface
10.0	236	0.720	290	0.889	3.76
15.0	158	0.483	296	0.906	1.86
19.91	120	0.367	304	0.931	0.94
25.0	96	0.296	316	0.965	0.37
30.0	82	0.250	330	1.010	0

TABLE 1. Parameters of the simulations of an incident sound wave train impinging on a Mach-4 slip surface. The wave train was incident at five angles, and three different amplitude trains were tested. For each angle the table lists the details of the zoning and the phase velocity of the wave fronts along the slip surface. Results of these simulations are shown in figures 1, 2, and 3.

Thus the AM analysis predicts that at an angle of 19.91° the incident sound wave train will excite the u_- kink mode. Symmetry considerations show that the u_+ kink mode will be excited by an identical sound wave train incident from the opposite side of the slip surface. Once formed, these kink modes are predicted to grow self-similarly in time. The AM analysis shows that there is no nonlinear mechanism for the formation of the u_0 mode, but that if the slip surface were given an initial kink this mode would also grow self-similarly.

4. Results

4.1. 5% R_+ *perturbation amplitude*

A series of numerical simulations was performed using a Mach-4 relative velocity slip surface with sound wave trains incident at five different angles. One angle was equal to the expected resonant angle of 19.91°, while the other angles were set to 10°, 15°, 25°, and 30° to bracket this resonant angle. The phase velocities of the incident sound waves along the slip surface are listed in table 1. As can be seen these velocities span a wide range around the resonant value. The amplitude of the sinusoidal perturbation in the R_+ Riemann invariant was set to 5% of the initial value in the adiabatic flow.

These five configurations were run to time $t = 2$. In this time the incident sound wave could travel 16 wavelengths, although in the actual calculations the interaction with the slip surface was finished by time $t \approx 0.75$. Movies of the dynamics of each simulation were produced using the Gould image display system at the University of Minnesota. The Gould system is capable of displaying raster images at 30 frames per second. It is a duplicate of much of the Ultra-Speed Graphics project at the Los Alamos National Laboratory (Winkler *et al.* 1987*a*, *b*). Repeated viewings of the movies with complete interactive control were vital to understanding the details of the fluid flow. Unfortunately these movies cannot be reproduced here, and it is necessary to display individual snapshots of the results.

The time evolutions of these simulations are presented in figures 1 (*a*)–1 (*g*), which display the five angles of incidence side by side to facilitate comparison. The figures are chosen to illustrate both the early and late history of the evolutions, and the times shown are $t = 0.24$, 0.36, 0.42, 0.60, 0.84, 1.04, and 2.0. In the figures the density is given a greyscale representation, with the higher densities appearing darker. In the first five figures a density of 0.29 is white, and a value of 1.98 is all

(a)

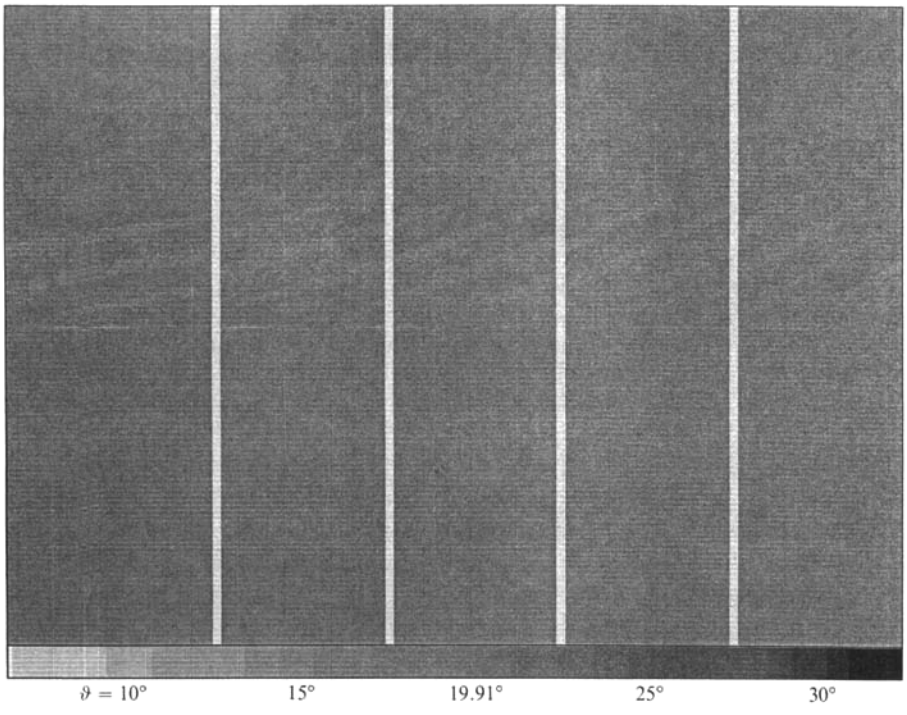

(b)

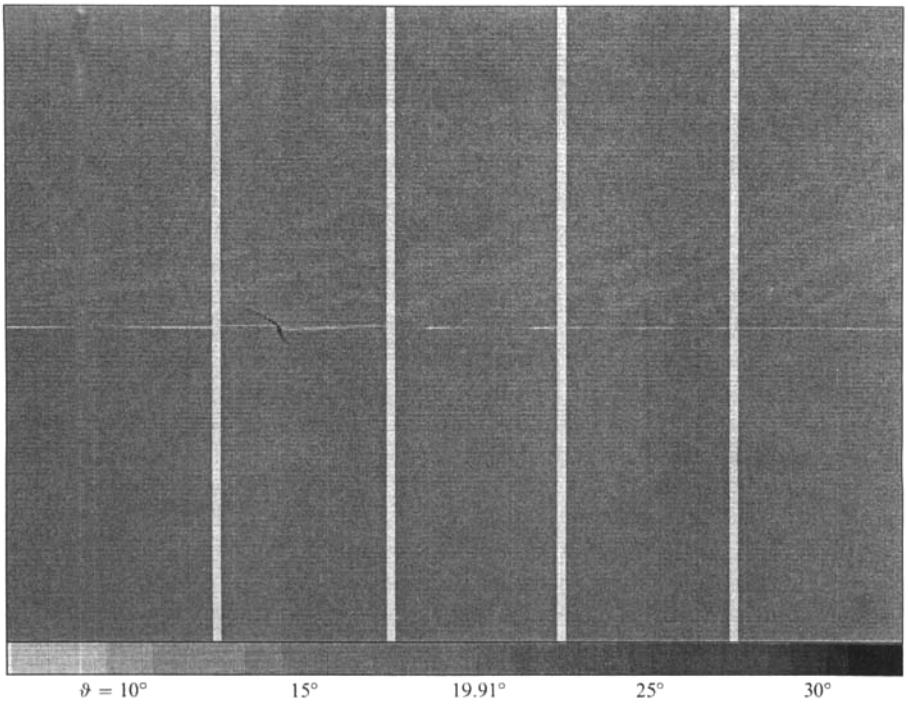

FIGURE 1 (a, b). For caption see page 109.

(*c*)

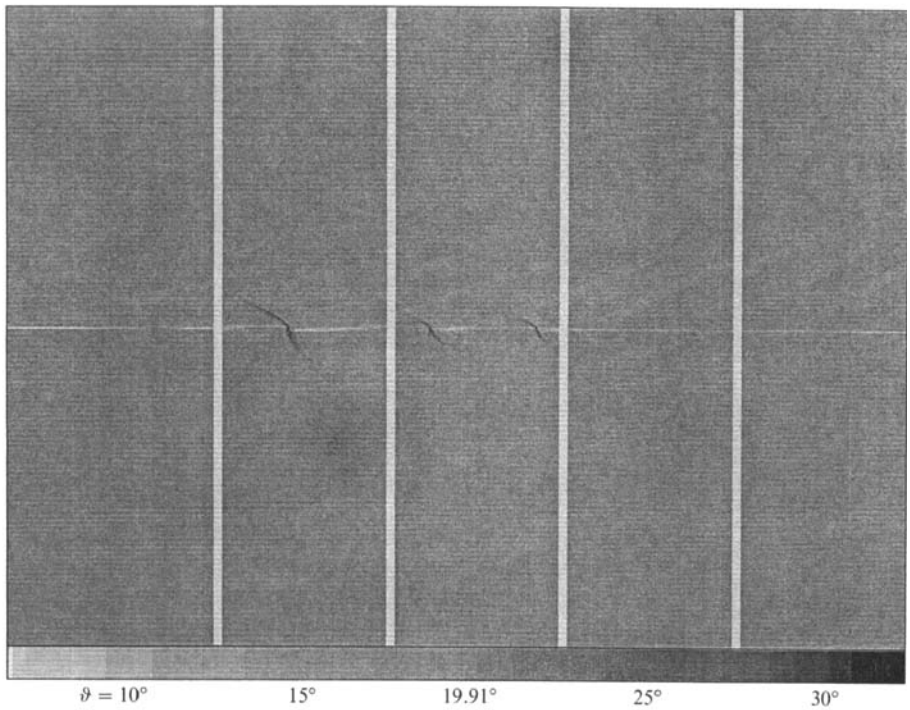

(*d*)

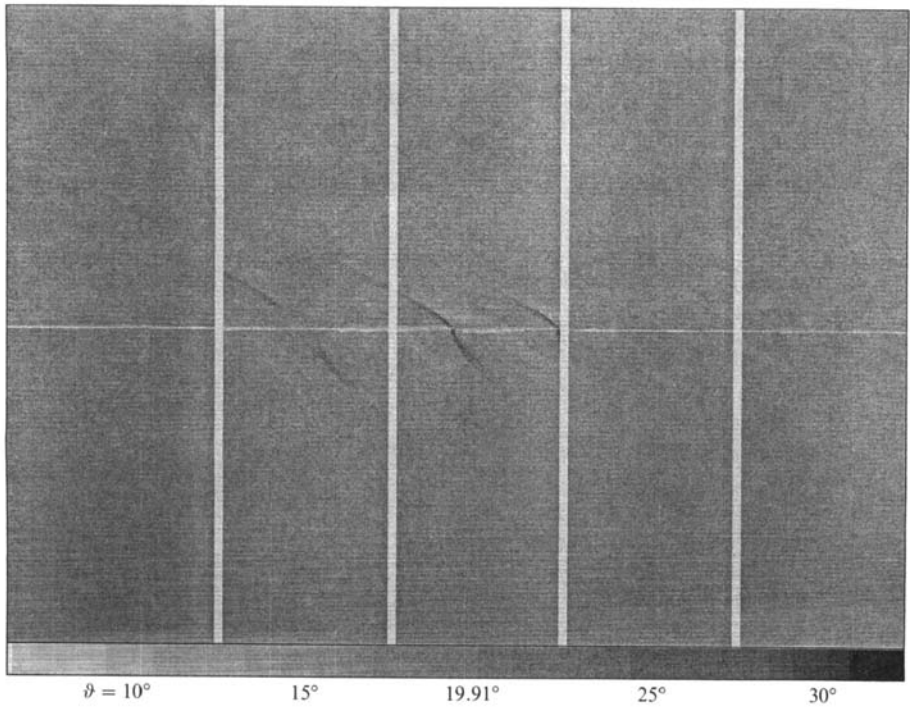

FIGURE 1 (*c*,*d*). For caption see page 109.

(e)

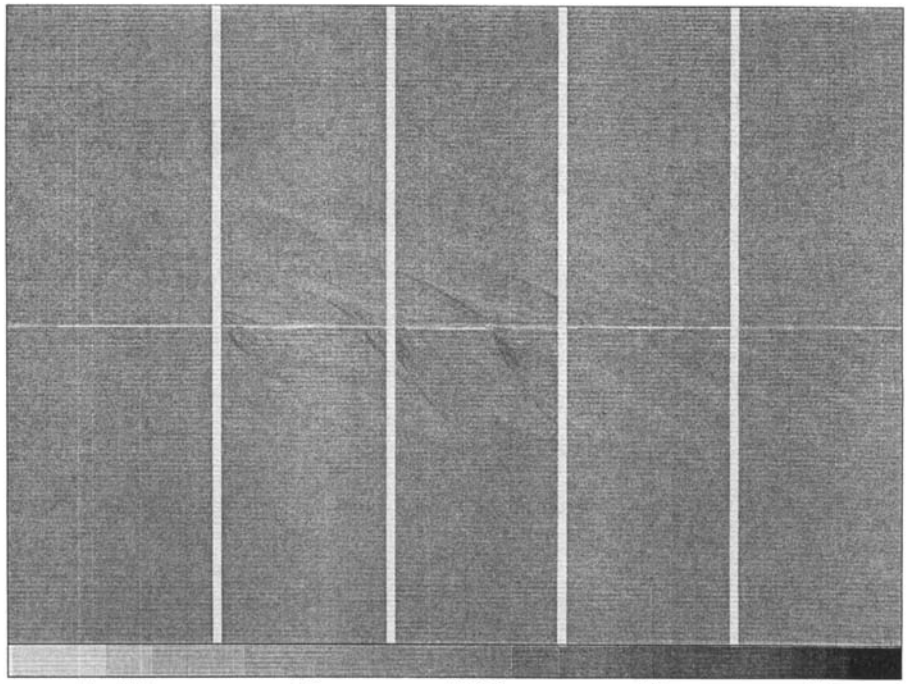

(f)

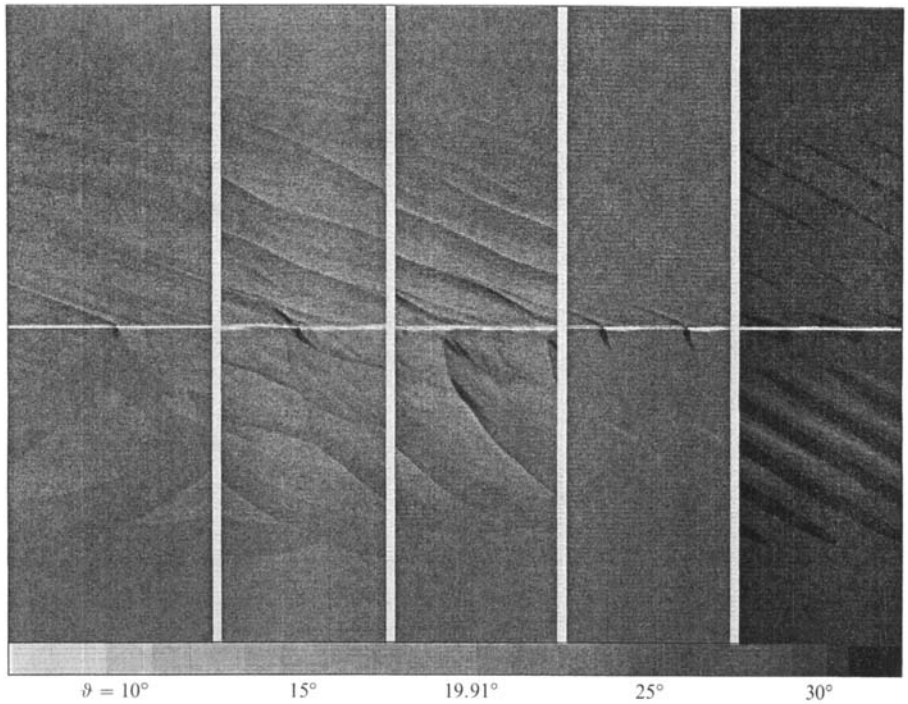

FIGURE 1 (*e*,*f*). For caption see facing page.

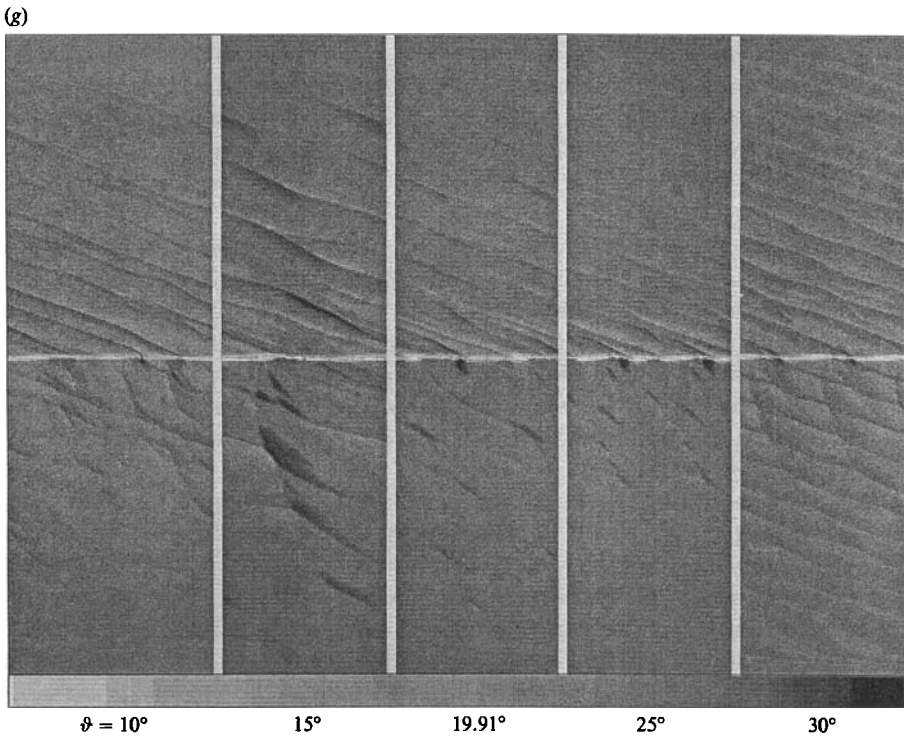

FIGURE 1. A comparison of the evolution of a Mach-4 equal-density slip surface interacting with five different incident sound wave trains. The different evolutions of the fluid density are presented side by side at identical times with the incidence angle of the sound waves displayed beneath. The wave trains were created by imposing a 5% sinusoidal perturbation in the R_+ Riemann invariant. The different simulations at time $t = 0.24$ are displayed in (*a*), while times $t = 0.36$, $t = 0.42$, $t = 0.60$, $t = 0.84$, $t = 1.04$, and $t = 2.0$ are shown in (*b–g*) respectively. The minimum and maximum densities displayed in the greyscale transfer function are 0.29 and 1.98, respectively. Additional details are described in the text.

black. For the other times the range between the maximum and minimum densities in each simulation was independently scaled to the full greyscale range. One period of the 10° simulation is displayed, and it shows 1.2, 1.6, 1.9, and 2.3 periods of the 15°, 19.91°, 25°, and 30° simulations, respectively.

The simulations begin similarly for all five angles of incidence. Because of the Gaussian envelope the sound waves do not reach the slip surface until time $t = 0.10$. As they begin to interact with the slip surface, some of the kinetic energy of the system is dissipated into heat. This heated gas expands, locally broadening the fluid interface. The broadening is greatest where the wave crests impinge on the slip surface, and thus has a period of $\lambda/\sin(\vartheta)$ along the interface. The incident waves have steepened into mild shocks by time $t \approx 0.24$ (figure 1*a*). After this time the slip surface responds differently to each incident wave train, and the rest of the evolutions will be presented separately.

4.1.1. $\vartheta = 19.91°$

The evolution of the predicted resonant angle simulation continues with the slip surface weakly reflecting and transmitting some of the incident waves. At time $t \approx 0.38$ (figure 1*c*, note that this is after similar behaviour is noted in the $\vartheta = 15°$ simulation) the slip surface develops a kink located at the trailing edge of the

broadened region of the slip surface. Note also that figure 1 (*c*) shows two kinks in the $\vartheta = 19.91°$ simulation because more than one period of the calculation is displayed. The kink is accompanied by shocks and rarefactions radiating into both sides of the slip surface. The kink and its nonlinear wave system move with a speed $\approx 0.4c$ in the direction of the incident waves' phase velocity. As it propagates the system grows nearly self-similarly until time $t \approx 0.50$, when two much smaller kinks appear in the slip surface.

The subsequent evolution of the flow is rather complex, and cannot be demonstrated adequately with time snapshots. One of the smaller kinks is disrupted when it is overtaken by one of the incident wave fronts. The disruption appears to create a very much weaker kink system which moves in the opposite direction from the others. It is identical to the other kinks and nonlinear wave systems in structure except that it is inverted, i.e. reflected about both the horizontal and vertical axes. The velocity of this oppositely moving kink is difficult to measure because it is so weak; an estimate is $-0.9c \pm 0.15c$.

Once this oppositely moving kink is generated the number of kink interactions increases significantly. In many such interactions oppositely moving kinks are created, and by time $t \approx 0.90$ the flow is dominated by collisions between oppositely moving kinks and their associated nonlinear wave systems. The incident sound waves have completed their interaction with the slip surface by time $t \approx 0.75$.

Much of the time history of this complicated flow can be discerned from the wave patterns radiated into the fluids on either side of the slip surface. These patterns are created by the shocks and rarefactions associated with the kinks as they move into the ambient fluids at approximately the local sound speed. The patterns therefore reflect the approximate peed of advance of the slip-surface kinks. Because the fluids on either side of the slip surface have equal and opposite velocities the kinks move with different velocities relative to each fluid. In this simulation the radiated wave patterns illustrate that the dominant kink systems vary in strength and speed, while several weaker systems propagate in both directions along the slip surface. The speed of most of the kinks is directly measured to be approximately 0.8 to 1.0, but speeds ranging from 0.4 to 1.3 were measured. After time $t \approx 1.0$ (figures 1*f* and 1*g*) the evolution of the slip surface is chaotic, although no large-scale bending of the flow has occurred. This is consistent with behaviour expected for a linearly stable flow.

4.1.2. $\vartheta = 25°$

In the 25° simulation the phase velocity of the incident waves along the slip surface is 0.37, in contrast to the predicted resonant value of 0.94. A kink begins to form in the slip surface at time $t \approx 0.6$ (figure 1*d*); however, because the phase velocity of the incident wave fronts is slower than the resonant value the full development of the kink is retarded by the applied perturbation.

The kink and nonlinear wave system begins a rapid acceleration when the incident fronts complete their interaction with the slip surface and the retarding influence leaves. By time $t \approx 0.9$ the kink system reaches a maximum velocity of $1.25 \pm 0.1c$. This acceleration can be discerned in the shock waves radiated from the interface (figure 1*e*). The kink subsequently slows to an average velocity of $0.9 \pm 0.1c$ as it grows in strength. During the kink acceleration and deceleration several new oppositely moving kink and wave systems are generated. These systems are much weaker than the initial kink, and move with a velocity of approximately $-0.9 \pm 0.15c$. These oppositely moving wave systems interact as in the 19.91° case, and a chaotic, but stable, flow ensues.

4.1.3. $\vartheta = 15°$

The 15° incident wave fronts have a phase velocity of 1.86c along the slip surface. This velocity is a little greater than twice the resonant value predicted by AM. The incident fronts heat the gas in the interface as before, and at time $t \approx 0.32$ (just before figure 1*b*) a kink appears at the trailing edges of these regions. The figures show that this kinking occurred earlier than in the 19.91° simulation. The kink appears approximately equidistant between the incident wave fronts. The incident fronts move at a velocity faster than the kink, which is moving at approximately 0.6c. At time $t \approx 0.4$ another weaker kink appears just ahead of an incident wave front and just behind the main kink system. This smaller kink moves in the same direction at a velocity of approximately 1.1c, and soon nearly catches up with the initial kink system. As it is about to do so, however, an incident wave front impinges on the region. At time $t \approx 0.54$ the existing kinks are completely disrupted and at least two weak kinks moving in the opposite direction are created. The disrupted kinks appear to regenerate themselves almost immediately.

The kinks continue to propagate and collide, heating the slip surface, which by time $t \approx 1.0$ (figure 1*f*) is several zones wide. The boundary of this heated gas is irregular, and periodically the kinks interact with the higher density gas protrusions into this layer. These protrusions also collide with each other. The result of the collisions is the generation of strong transient kinks that are quickly disrupted by new interactions. The transient kinks are stationary during their lifetimes, as evidenced by the symmetric shocks that they send into the gas on either side of the slip surface.

4.1.4. $\vartheta = 10°$

The phase velocity of the incident wave front in the 10° simulation is 3.70. This large phase velocity is supersonic with respect to both fluids. The incident sound waves result in a heating and broadening of the slip surface that is greater and more uniform than in the other cases. When the incident sound waves complete their interaction the slip surface kinks weakly. The kinking is clearly not directly related to the perturbation supplied by the incident sound waves.

The kink and nonlinear wave system grow in strength and by time $t \approx 1.1$ are well defined. The kink is generated at a velocity of approximately 1.1c, but slows to 0.9c as its strength increases. Also at time $t \approx 1.1$ very weak kinks appear at four other locations along the slip surface, and one of these kinks moves in the opposite direction. The velocity is again approximately $0.9 \pm 0.1c$. The ensuing interactions are very similar to those observed in the other simulations, and by time $t = 2$ (figure 1*g*) the evolution is chaotic.

4.1.5. $\vartheta = 30°$

The incident wave fronts in the 30° simulation have a zero phase velocity along the slip surface. The result of the interaction is that the incident waves are merely transmitted and reflected while the slip surface remains unperturbed. Again it is not until after the incident waves have been completely reflected and transmitted that the slip surface kinks in several locations. The strongest of the kinks moves forward at a velocity of approximately $1.1 \pm 0.1c$, while more numerous and weaker kink systems move in the opposite direction at $0.9 \pm 0.1c$. The ensuing interactions eventually disrupt the forward-moving kink and others which follow, and as in the 15° simulation these kink collisions produce transient, stationary kink systems. By

time $t = 2$ (figure 1*g*) forward- and backward-moving kink systems exist in approximately equal numbers, although the forward systems are somewhat stronger.

4.2.1. 1% R_+ *perturbation amplitude*

To explore the dependence of the incident sound wave train amplitude on the above results, three simulations were run with the perturbation amplitude of the R_+ Riemann invariant set to 1%. The angles of incidence were 15°, 19.91°, and 25°. The simulations were calculated to $t = 1.0$. The details of the zoning were the same as listed in table 1 for the 5% R_+ perturbation runs. Figure 2(*a–c*) displays the time evolution of these more mildly perturbed slip surfaces. The format is the same as in figure 1, and the times shown are $t = 0.60$, 0.84, and 0.96. The initial conditions (not shown) are very similar to figure 1(*e*), except that the amplitude of the incident sound waves is approximately 5 times smaller. The density displayed ranges from 0.28 to 2.01.

In the 19.91° and 15° cases behaviour similar to the 5% R_+ perturbation simulations is observed, except that it occurs at later times. For the 15° simulations the 1% perturbation caused the slip surface to kink at time $t \approx 0.45$, compared with $t \approx 0.3$ for the 5% R_+ perturbation. The corresponding times for the 19.91° case are $t \approx 0.7$ and $t \approx 0.3$. The 25° incidence angle, however, now shows no significant nonlinear development. This simulation is very similar to the early (i.e. to time $t =$ 1.0) evolution of the 30° incidence angle with the 5% R_+ perturbation. The incident wave train is partially transmitted and reflected, and by time $t = 1.0$ the slip surface has not shown nonlinear kink development. The slip surface has, however, been significantly widened by the waves' passage. It might be expected that eventually the surface would kink as the slip surface in the 30° angle 5% R_+ perturbation simulation did once the incident sound wave train had passed.

4.3. 50% R_+ *perturbation amplitude*: $\vartheta = 30°$

The effects of increasing the amplitude of the incident sound wave train were explored by running the 30° incidence angle case with a very large 50% perturbation in the R_+ Riemann invariant. For reference, a 5% R_+ perturbation at this incidence angle did not excite the kink modes. The results of the evolution to time $t = 1.0$ are displayed in figures 3(*a*) and 3(*b*). The format of these figures is different than the others, in that the time increases from left to right within each figure. The time interval is $\Delta t = 0.1$. Figure 3(*a*) displays times $t = 0.1$ to 0.5, and figure 3(*b*) continues with times $t = 0.6$ to 1.0.

With this large initial perturbation the incident sound waves steepen to strong shocks almost immediately. The large amplitude of the perturbation means that the two families of Riemann invariants can no longer be excited independently, and therefore a weaker wave system moving in the opposite direction is also generated. When the incident wave train reaches the slip surface the interface kinks promptly and violently. Interestingly, the kink modes excited by this strong perturbation move in the direction opposite to that of the kinks created initially in the other cases. The amplitude of the bend generated in the slip surface is much greater than for any of the 5% R_+ perturbation simulations.

4.4. 5% R_+ *perturbation amplitude*: $\vartheta = 18.67°$

In a very preliminary exploration of the width of the nonlinear resonance, a simulation with the wave train incident at an angle of 18.67° was performed. At this angle the phase velocity of the perturbation along the slip surface was 1.12*c*, 20%

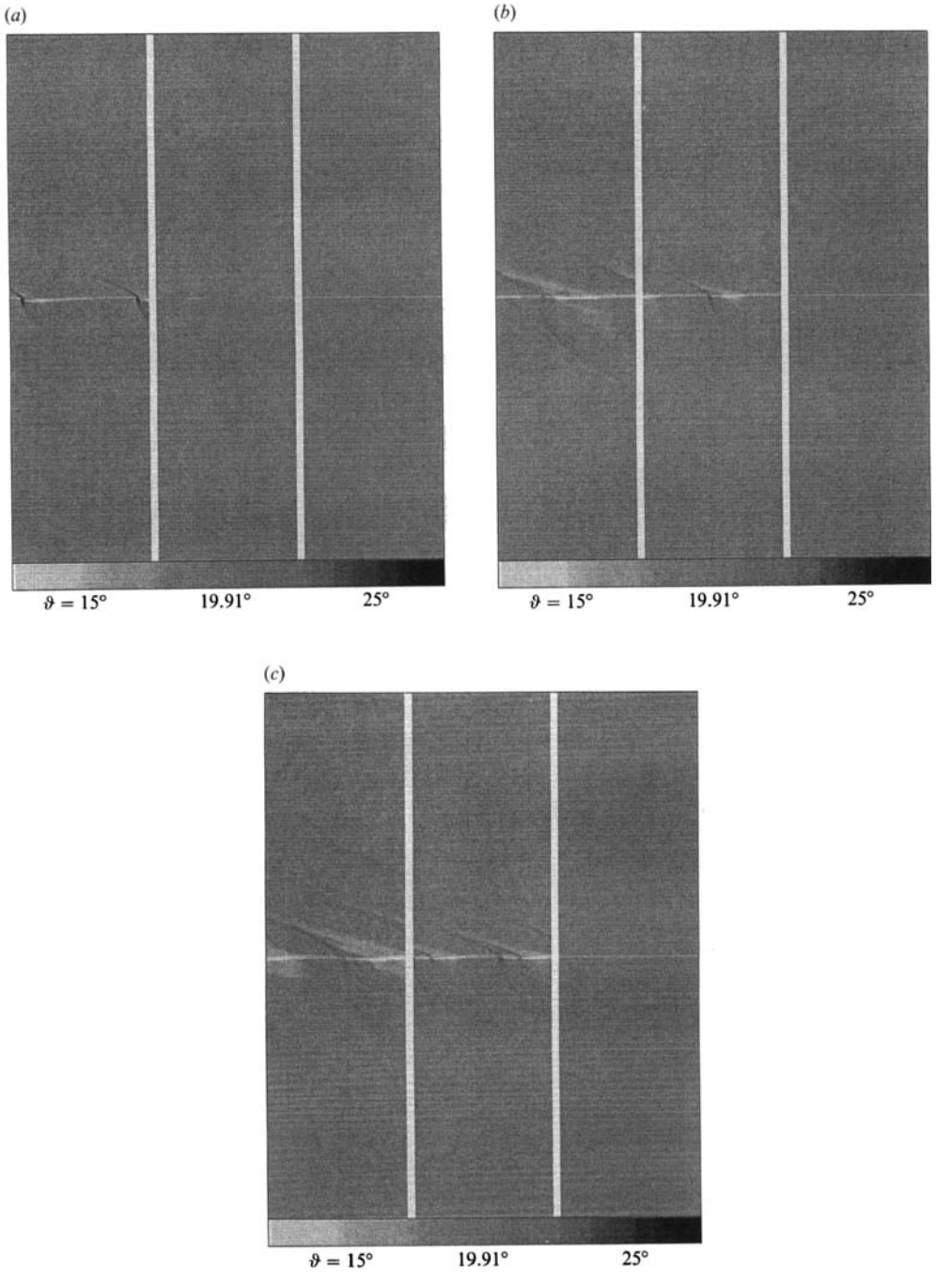

FIGURE 2. A comparison of the evolutions of a Mach-4 equal-density slip surface interacting with three different incident sound wave trains. In this figure the incident wave trains are approximately 5 times weaker than in figure 1, and were created by imposing a 1% sinusoidal perturbation in the R_+ Riemann invariant. The different evolutions of the fluid density are presented side by side at identical times, with the incidence angle of the sound waves displayed beneath. The different evolutions at times $t = 0.60$, $t = 0.84$, and $t = 0.96$ are displayed in (a–c) respectively. The minimum and maximum densities displayed in the greyscale transfer function are 0.28 and 2.01, respectively. Additional details are described in the text.

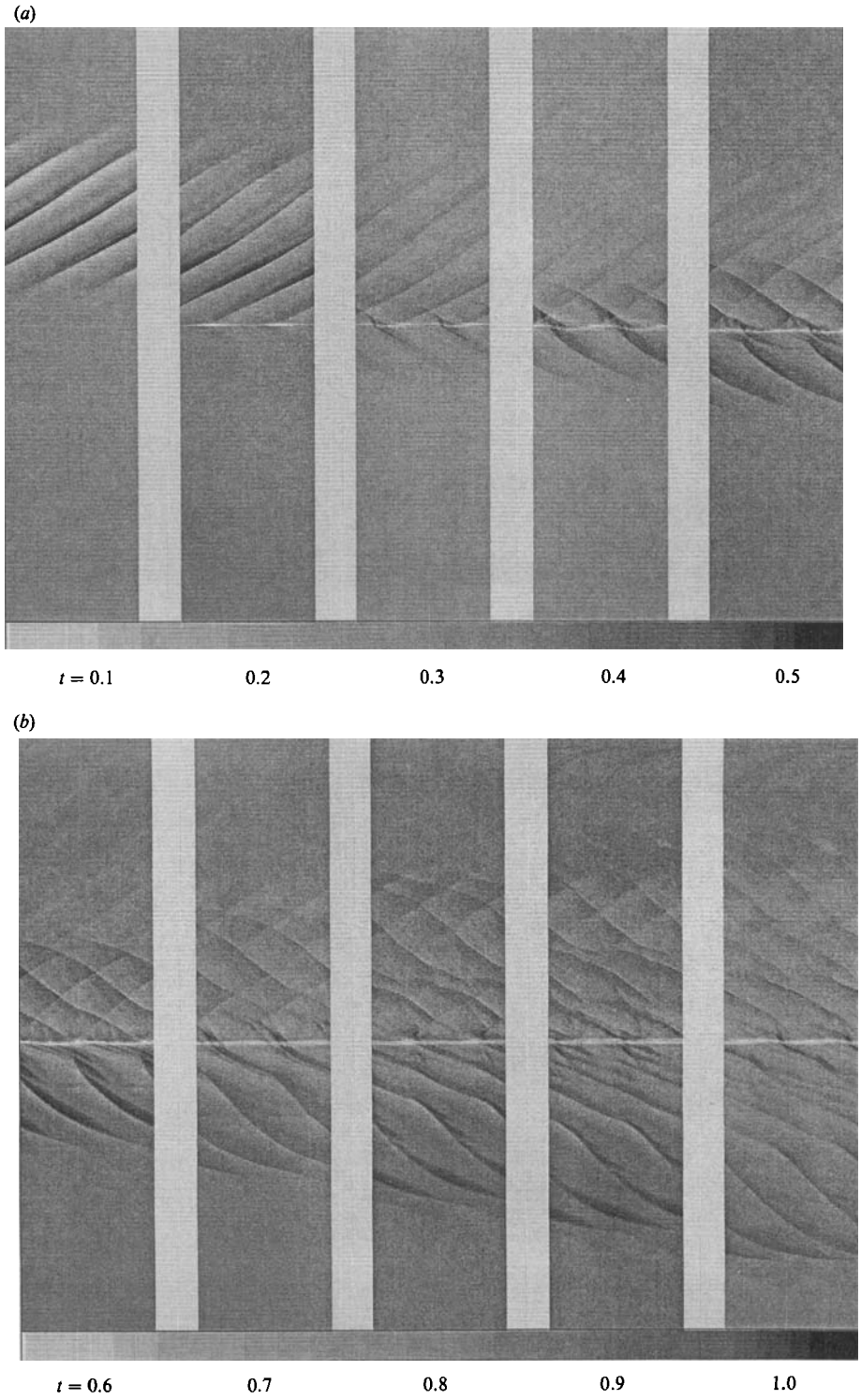

FIGURE 3(*a*, *b*). The time evolution of a Mach-4 equal-density slip surface interacting with a strongly nonlinear train of sound waves incident at an angle of 30°. Time increases from left to right as shown. The incident wave train was created by imposing a 50% sinusoidal perturbation in the R_+ Riemann invariant. Additional details are described in the text.

higher than the predicted resonant value. The amplitude of the R_+ perturbation was 1%. The slip surface kinks very similarly to the 19.91° case. but at time $t \approx 0.5$. This time is actually ≈ 0.2 earlier than in the simulation at the predicted resonant angle.

4.5. *Higher resolution* 19.91° *with* 5% R_+ *perturbation amplitude*

The broadening of the slip surface seen in the above simulations is a result of energy dissipation of numerical origin, since when two fluids are mixed within a computational zone they are given identical velocities. This velocity reassignment conserves momentum and total energy, and it increases the internal energy at the expense of the kinetic energy. To test if the broadening of the slip surface affects the formation and propagation of the kink modes, the 19.91° angle of incidence case was calculated with twice the resolution of the above simulations. The extent of the problem was the same as discussed above except that the size of the computational area was 240 by 1440 zones. Slip-surface broadening of purely numerical origin will be half as wide as in the more coarsely zoned simulation. The problem was calculated to $t = 1.74$. Snapshots of the evolution are presented in figure 4(*a–d*).

The evolution begins as in the lower-resolution simulation, and the slip surface forms a single kink and nonlinear wave system at time $t \approx 0.32$. This time is nearly equal to the previous time of kink formation, which was at time $t \approx 0.38$. The evolution of the slip surface during the period of interaction with the incident sound waves is very similar to that calculated on the coarser grid; however, dramatic differences appear later. The instability of the slip surface is much greater than in the coarser resolution calculation. By time $t \approx 0.8$ small-scale Kelvin–Helmholtz rolls appear along the interface and dominate the kink modes. This behaviour is not present in the coarser resolution run, even by the end of the calculation. Clearly, the amount of numerical viscosity strongly influences the nature of the flow. More work will be necessary to explore this dependence.

5. Discussion

The simulations presented above have explored the response of a Mach-4 equal-density slip surface to a variety of impinging sound wave trains. The results show the existence of a resonance in the response of the slip surface as the angle of incidence of the sound waves is varied. This resonance was predicted by the stability analyses of Miles (1957) and AM, which showed that at resonance the amplitude of the reflected waves is much greater than the incident wave amplitude. The PPM simulations show that when the incident wave amplitude is 5% in the R_+ Riemann invariant, the 15°, 19.91°, and 25° incident-angle wave trains excite the nonlinear kink response in the slip surface, and the reflected waves are strong shocks. For the other two angles of incidence the slip surface does not display nonlinear behaviour until after the incident trains have finished their interactions.

The width of the resonance becomes narrower as the strength of the incident sound waves is decreased. For a 1% perturbation in R_+ the 25° incidence-angle wave train no longer excites the kink modes, and the sound waves are reflected without amplification. The waves incident at 15° still produce strongly nonlinear behaviour. It is possible that this perturbation excites the kink modes because the phase velocity of the wave fronts along the slip surface is very nearly equal to twice the resonant value. The possibility of harmonic excitation was not discussed by AM, however. The width of the resonance is at least 20% in phase velocity space since the 1% R_+ perturbation wave train at an 18.7° angle of incidence also produces kinks.

(a)

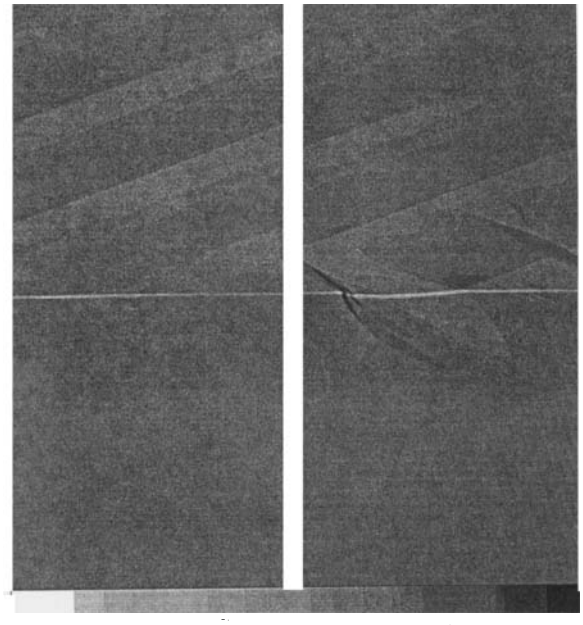

$t = 0.3$ 0.4

(b)

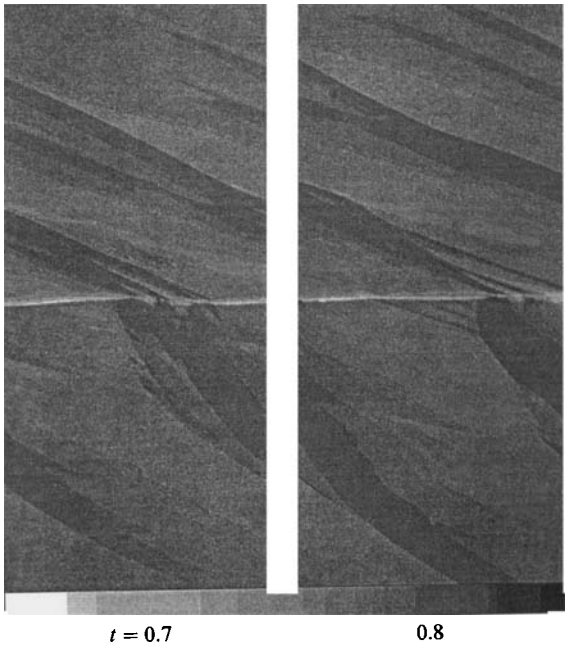

$t = 0.7$ 0.8

FIGURE 4. For caption see facing page.

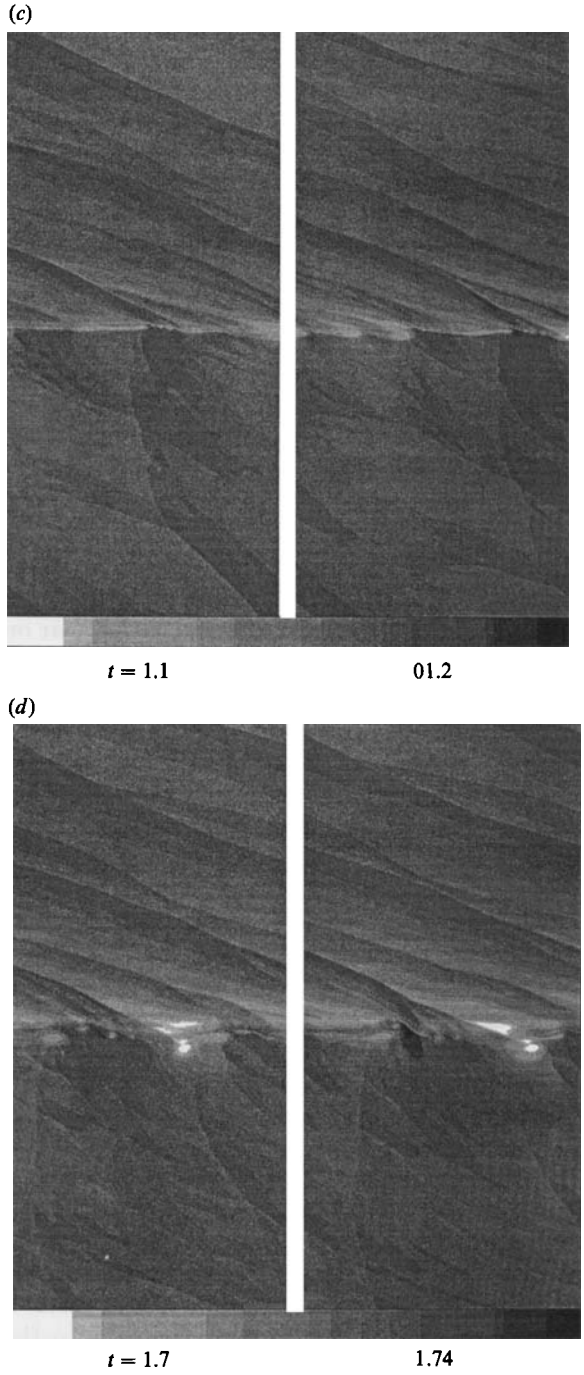

FIGURE 4(*a–d*). The high-resolution time evolution of a Mach-4 equal-density slip surface interacting with a train of sound waves incident at an angle of 19.91°. Time increases from left to right as shown. The incident wave train was created by imposing a 5% sinusoidal perturbation in the R_+ Riemann invariant. The minimum and maximum densities displayed in the greyscale transfer function are 0.27 and 1.99, respectively. The simulation was calculated using an extremely fine grid of 1440×240 zones, twice the resolution of the results presented in figures 1–3.

The nature of the kink modes observed in the fully nonlinear simulations are both qualitatively and quantitatively similar to those discussed by AM, yet some differences exist. The kink modes observed in these simulations move in both directions at the speed predicted by AM. Even kinks excited by a perturbation with the wrong phase velocity, such as in the 25° incidence-angle 5% R_+ simulation, will, once the retarding perturbation is removed, quickly reach this characteristic velocity. Speeds different than the predicted value are observed, however. Given the complex and strongly nonlinear interactions which occur in the flows this disagreement is not too serious, since the AM analysis included only weakly nonlinear effects.

A fundamental difference between the AM kink modes and those observed in the simulations is that the analytical kinks are presented as simple bends in the slip surface. It is not clear in this picture how the slip surface returns to its initial orientation, as it obviously must to form an isolated distortion in an otherwise unperturbed interface. The answer to this distinction may also lie in the less than fully nonlinear nature of the analytical work.

Only the propagating kink modes, those designated $u_\pm$ by AM, were clearly observed in these simulations. These kink modes may be related to the travelling wave modes discussed by Blumen, Drazin & Billings (1975), Drazin & Davey (1977), and Roy Choudhury & Lovelace (1984), although the latter modes are derived using linear stability analyses of finite-width shear layers with linear or hyperbolic tangent velocity profiles, instead of the vortex sheet as in the AM analysis. The relationship among these different analyses is presently unclear.

A well-defined stationary u_0 mode was not observed in these simulations; however, transient stationary features with symmetric nonlinear wave systems were sometimes created in the interaction of the propagating kink modes. Based on the behaviour seen in early equal-density Mach-4 slip surfaces, it is possible that these stationary features will begin to dominate the flow at much later times. Such a feature at time 19 is displayed as the last frame in figure 8 of Woodward *et al.* (1987). The development of this instability may arise because a well-resolved shear layer has developed out of the initial slip surface as a result of the propagating kink interactions, and for which the analyses mentioned above are appropriate. It will be necessary to evolve the simulations to much later times to test this idea.

5.1. *Implications for jet stability*

These simulations of the basic kink mode in supersonic slip surfaces have important implications for the understanding of supersonic jet stability. Woodward (1986) and Woodward *et al.* (1987) have performed PPM simulations of two-dimensional Mach-2 jets in Cartesian geometry. In this geometry a jet is simply two plane-parallel slip surfaces, the width of the jet being the distance between the slip surfaces. The simulations show that the stationary kink mode generates a resonance in the large-scale bending or meandering properties of the jet. At Mach-2, stationary kinks created on opposite sides of the jet send oblique shocks into the jet interior which ultimately interact with the jet boundary on the opposite side. The interaction creates a kink in the jet wall and the shock is reflected back to the other side of the jet. If the width of the jet and the angle of the reflected shock are properly matched, the reflected shock will reinforce the initial kink, and the pattern will reinforce itself. The result of this resonance is the creation of a large bend in the jet.

This bending or meandering is very disruptive in the simulations that have odd symmetry. In three dimensions the analogue of this two-dimensional instability is

the helical mode. When the jet is given even symmetry by applying a reflecting boundary condition along the jet axis, the initial oblique shocks reflect at the jet axis via either regular or Mach reflection. The response of the jet in this case is to pinch, analogous to the three-dimensional pinch or sausage mode.

When the kink modes generated in the jet boundary are propagating instead of stationary, as in the initial evolution of a Mach-4 slip surface, the resonance described above will not occur. Only after the long time necessary for the stationary modes to dominate the flow will a large-scale bending of the jet develop. Thus the nature and dynamics of the basic kink modes relates simply and directly to the stability of jets.

The effect on jet stability of a resonance involving oblique shocks generated by finite-amplitude kinks in the jet boundaries was not fully appreciated by previous linear stability analyses because shocks are fundamentally nonlinear processes. The AM analysis is less restrictive because it includes small-amplitude nonlinear effects. By verifying the fundamental ideas of their analysis of the basic kink modes, the present numerical work will allow researchers to proceed with confidence in applying analytical similar techniques to more complex geometries in higher dimensions. These nonlinear analyses should permit initial explorations of the stability of three-dimensional cylindrical jets. They may isolate interesting regions of parameter space which can then be studied in the fully nonlinear limit using the much more time-consuming numerical simulations. These simulations are at present too expensive to use in an unguided exploration of all of parameter space.

6. Summary

The response of a Mach-4 equal-density slip surface to a variety of impinging sound wave trains was numerically simulated using PPM. The initial conditions were designed to match the problem analytically analysed by Artola & Majda (1987). The results confirm the existence of a resonance in the response of the slip surface. When the amplitude of the perturbation in the appropriate Riemann invariant is 5%, the angles of incidence closest to the predicted resonant angle excite nonlinear behaviour in the slip surface. At these angles the amplitude of the reflected waves is much greater (i.e. a shock) than the incident wave amplitude. The observed resonance is fairly broad, but as the strength of the incident waves is reduced the resonance narrows.

The nature of the nonlinear kink modes observed in the simulations is similar to that discussed by AM. Most of the modes move in either direction with speeds near the predicted value. Speeds of other than this value are observed, but the disagreement is not serious in view of the strongly nonlinear behaviour which is seen in the simulations but is not treated by the AM analysis. The stationary modes discussed by AM are perhaps observed as transient structures. It is suggested that they will eventually dominate the flow at much later times. The role of the kink modes in the stability of slab jets is discussed, and it is argued that the stationary modes are more disruptive than the propagating kink modes.

The above simulations were performed using the Cray 2 at the Minnesota Supercomputer Center. The authors acknowledge generous grants of computer time, and would like to thank the staffs of the MSC and the Minnesota Supercomputer Institute for help with the computations.

Support for numerical simulations of supersonic gas dynamics by P.R.W. at the

University of Minnesota is provided by Office of Energy Research of the Department of Energy, under contract DE-FG02-87ER25035, by the National Science Foundation through grant AST-8611404, and by the Air Force Office of Scientific Research through an equipment grant AFOSR-86-0239. Support for the graphics equipment vital to this project was also provided by the University of Minnesota, Gould, Inc., and Sun Microsystems. Support for J.P. was provided by the NSF through grants AST83-15949 to T. W. Jones and L. Rudnick and AST86-11404 to P. R. Woodward.

Movies of the above simulations can be obtained by sending a blank VHS or $\frac{3}{4}$ inch U-Matic videotape with return postage to P.R.W at the Minnesota Supercomputer Institute.

REFERENCES

ARTOLA, M. & MAJDA, A. J. 1987 *Physica D* **28**, 253 (referred to herein as AM).

BLUMEN, W., DRAZIN, P. G. & BILLINGS, D. F. 1975 *J. Fluid Mech.* **71**, 305.

BRIDLE, A. H. & PERLEY, R. A. 1984 *Ann. Rev. Astron. Astrophys.* **22**, 319.

COLELLA, P. & WOODWARD, P. R. 1984 *J. Comput. Phys.* **54**, 174.

COURANT, R. & FRIEDRICHS, K. O. 1948 *Supersonic Flow and Shock Waves.* Interscience.

DRAZIN, P. G. & DAVEY, A. 1977 *J. Fluid Mech.* **82**, 255.

GERWIN, R. A. 1968 *Rev. Mod. Phys.* **40**, 652.

GODUNOV, S. K. 1959 *Mat. Sb.* **47**, 271.

HJELLMING, R. M. & JOHNSTON, K. J. 1985 In *Radio Stars* (ed. R. M. Hjellming & D. M. Gibson), p. 309. Reidel.

LADA, C. 1985 *Ann. Rev. Astron. Astrophys.* **23**, 267.

LEER, B. VAN 1979 *J. Comput. Phys.* **32**, 101.

MILES, J. W. 1957 *J. Acoust. Soc. Am.* **29**, 226.

MILES, J. M. 1958 *J. Fluid Mech.* **4**, 538.

ROY CHOUDHURY, S. & LOVELACE, R. V. E. 1984 *Astrophys. J.* **283**, 331.

WINKLER, K.-H. A., CHALMERS, J. W., HODSON, S. W., WOODWARD, P. R. & ZABUSKY, N. J. 1987*a* *Phys. Today* **40**, 28.

WINKLER, K.-H. A., HODSON, S. W., CHALMERS, J. W., MCGOWEN, M., TOLMIE, D. E., WOODWARD, P. R. & ZABUSKY, N. J. 1987*b* *Cray Channels* **9**, 4.

WOODWARD, P. R. 1985 In *Numerical Methods for the Euler Equations of Fluid Dynamics* (ed. F. Angrand, A. Dervieux, J. A. Desideri & R. Glowinski), p. 493. Philadelpha: SIAM.

WOODWARD, P. R. 1986 In *Astrophysical Radiation Hydrodynamics* (ed. K.-H. A. Winkler & M. L. Norman), p. 245. Reidel.

WOODWARD, P. R. & COLELLA. P. 1984 *J. Comput. Phys.* **54**, 115.

WOODWARD, P. R., PORTER, D. H., ONDRECHEN, M., PEDELTY, J., WINKLER, K.-H., CHALMERS, J. W., HODSON, S. W. & ZABUSKY, N. J. 1987 *Science and Engineering on Cray Supercomputers*, p. 557. Minneapolis: Cray Research, Inc.